The Numerical Representation of Entrainment in Parameterizations of Boundary Layer Turbulent Mixing

A. P. LOCK

Met Office, Bracknell, Berkshire, United Kingdom

(Manuscript received 28 April 2000, in final form 12 October 2000)

ABSTRACT

Problems have been identified with parameterizations of convective boundary layers, in particular with their numerical treatment of the capping inversion. It is shown that the turbulence scheme can combine with the numerical representation of subsidence to produce unphysical entrainment, as was also identified by Lenderink and Holtslag. A correction is proposed for the Lock et al. boundary layer parameterization in which a discontinuous inversion is diagnosed from the mean thermodynamic profiles every time step. This then allows a consistent treatment of subgrid-scale processes in the region of the inversion. In particular, the parameterized turbulent entrainment flux can be adjusted to allow for the spurious entrainment arising from the conflicting representations of turbulent mixing and vertical advection. It also allows a direct coupling between the turbulent and radiative fluxes to ensure that cloud-top radiative cooling is correctly distributed between the inversion grid level and the mixed layer.

The revised scheme demonstrates a much improved representation of stratocumulus-capped boundary layers, not only in single-column model tests but also in a climate-resolution GCM. In the latter, the semipermanent subtropical stratocumulus sheets appear realistic, both in terms of their cloud amount and their evolution. This suggests that a significant cause of the lack of stratocumulus in many GCMs may not be the inaccuracy of the parameterizations employed, but rather their numerical implementation.

1. Introduction

In a convective boundary layer, buoyancy-driven thermals constantly overturn the air, keeping the layer well mixed and profiles of conserved variables approximately uniform with height. Modeling the evolution of such variables in the vertical column of a general circulation model (GCM) is then the deceptively simple task of applying the upper and lower boundary conditions, given that more or less accurate parametrizations of these have now been developed (be they either explicit or implicit in the turbulence closure scheme). Recent work by Lenderink and Holtslag (2000), however, suggests there are problems with the numerical treatment of inversions by boundary layer mixing schemes when the free troposphere is subsiding (as is usually the case for stratocumulus-capped boundary layers). In single-column model (SCM) stratocumulus simulations with their *E–l* turbulence scheme, they found the numerical representation of subsidence combined with the turbulence scheme to produce unphysical ''numerical'' entrainment. As will be shown in section 3, precisely the same problem has been found with the specified eddy diffusivity profile scheme of Lock et al. (2000). GCM tests with that scheme, described in Martin et al. (2000), demonstrated realistic boundary layer structure in the subtropical stratocumulus areas but with a large deficit in cloud amount. As will be discussed, it would appear that a significant cause of that lack of stratocumulus may not be the inaccuracy of the parametrizations employed, but rather their numerical implementation and how the entrainment parametrization, in particular, interacts with other schemes in the model.

The boundary layer scheme, based on that of Lock et al. (2000), is briefly described in section 2 and a simple example illustrating the problem of spurious numerical entrainment is given in section 3. A method for significantly reducing these problems is introduced in section 4. It is similar to that in Grenier and Bretherton (2001) and is based on ideas from B. Stevens (2000, personal communication), introduced in Stevens et al. (1999). Realistic assumptions are made about the subgrid-scale structure of the top part of the mixed layer and capping inversion, so that the parametrized turbulent fluxes can be represented on the finite difference grid in a manner that is consistent with large-scale advection and cloud-top radiation. SCM and GCM results are presented in sections 5 and 6, respectively.

Corresponding author address: Dr. A. P. Lock, Rm 172, Met Office, London Road, Bracknell, Berkshire RG12 2SZ, United Kingdom.
E-mail: aplock@meto.gov.uk

2. The original scheme

The Lock et al. (2000) boundary layer mixing scheme is a first-order closure. It is formulated in the moist variables θ_ℓ, the liquid/frozen water potential temperature, and q_t, the specific total water content. It combines a local, Richardson number–based, calculation of the eddy diffusivities [K(Ri), as in Smith (1990)], predominately for stable boundary layers, with nonlocally determined K profiles for convective boundary layers. The latter have a prescribed shape over the diagnosed depth of the mixed layer and their magnitudes are related to a turbulent velocity scale that is determined from the forcing. There are two profiles, one (K^{surf}) representing turbulence driven from the surface (by both shear and buoyancy production) and the other (K^{Sc}) representing buoyancy production of turbulence from cloud top by both radiative and evaporative processes. The vertical flux of a quantity χ is given by

$$\overline{w'\chi'} = -\max[(K_\chi^{\text{surf}} + K_\chi^{\text{Sc}}), K_\chi(\text{Ri})]\frac{\partial\overline{\chi}}{\partial z} + K_\chi^{\text{surf}}\gamma_\chi, \quad (1)$$

where K_χ is the appropriate diffusivity (K_m for momentum, K_h for scalars) and the prime denotes deviation from the horizontal mean indicated by an overbar. The last term on the right-hand side represents a nonlocal flux. Currently it is only related to surface forcing and is nonzero only for $\chi = \theta_\ell$, in which case the countergradient term, γ_{θ_ℓ}, is calculated as in Holtslag and Boville (1993). The presence and depth of convectively unstable surface-driven mixed layers is determined from a moist adiabatic parcel ascent. Additionally, entrainment at the top of well-mixed layers is parametrized directly using the scheme of Lock (1998), as will be discussed further in section 3b.

Finally, in determining the vertical extent of the K^{surf} and K^{Sc} profiles, the scheme makes two explicit diagnoses. The first is of the presence of cumulus convection. As described in Lock et al., this is diagnosed when the ratio of the gradient of $\overline{q_t}$ between the top of the parcel ascent and the lifting condensation level (LCL) to that between the LCL and the surface is greater than a certain threshold. If cumulus convection is diagnosed, the top of K^{surf} is set to the height of the LCL (rather than the inversion). This is so that mixing through the cumulus cloud layer is carried out by the model's mass-flux convection scheme and not by the eddy viscosity–based boundary layer scheme.

The second is of the depth of cloud-top driven mixing that enables turbulent mixing in both well-mixed and decoupled stratocumulus layers to be modeled. There is an important difference in the method of this diagnosis between the boundary layer scheme used in this study, and referred to as the standard (SBL) scheme, and that described in Lock et al. Here, the vertical extent of turbulent mixing driven from cloud top is diagnosed, following Turton and Nicholls (1987), based on the buoyancy production and consumption of turbulent kinetic energy (TKE) within the layer. The buoyancy flux at grid-level heights $z_{k+1/2}$, resulting from the specified K_h^{Sc} profile to a depth z_{ml} below cloud top, is calculated as

$$\overline{w'b}|_{z_{k+(1/2)}} = -K_h^{\text{Sc}}|_{z_{k+(1/2)}} \times g\left\{[(1 - C_F)\beta_T + C_F\tilde{\beta}_T]\frac{\Delta_{k-1}\overline{\theta_\ell}}{\Delta_{k+1}z} + [(1 - C_F)\beta_q + C_F\tilde{\beta}_q]\frac{\Delta_{k+1}\overline{q_t}}{\Delta_{k+1}z}\right\}, \quad (2)$$

where β_T, β_q, $\tilde{\beta}_T$, and $\tilde{\beta}_q$ are buoyancy parameters (given in Lock et al. 2000); C_F is the cloud fraction; and Δ_k denotes the k to $k - 1$ grid-level difference. An iterative method is then used to find the greatest z_{ml} that keeps the magnitude of buoyancy consumption of TKE within the mixed layer less than a tenth of the buoyancy production [the factor being an empirical observation from the large eddy simulations described in Lock (1998)]. If the K_h^{Sc} profile does not extend to the surface in a layer originally identified from the parcel ascent as well mixed, decoupling is deemed to have occurred. The appropriate height for the top of the K_h^{surf} profile is then diagnosed using the same condition on the TKE budget, but with the buoyancy flux profile in (2) calculated using $K_h^{\text{surf}} + K_h^{\text{Sc}}$, keeping K_h^{Sc} fixed. Note that this method cannot explicitly force decoupling because it relies on the mean thermodynamic profiles to calculate the buoyancy flux. The formulation of a predictive parameterization is hampered by the current lack of understanding of this important process. The previous diagnosis of decoupling (determined from adiabatic parcel descents) has been found to be insufficiently robust and somewhat time step dependent, as was discussed in Lock et al.

3. A delicate balance

As a simple illustration of the problem described by Lenderink and Holtslag (2000) as numerical entrainment, this section will consider the balance between subsidence and turbulent entrainment at the top of a convective boundary layer and, in particular, how this is represented numerically in boundary layer mixing schemes.

a. The balance in "reality"

For most of this analysis, horizontal advection and "physics" processes other than turbulent mixing will be ignored (radiative processes will be introduced later). The equation for the time variation of q_t can then be written

$$\frac{\partial q_t}{\partial t} = -w_S\frac{\partial q_t}{\partial z} - \frac{\partial}{\partial z}(\overline{w'q_t'}), \quad (3)$$

where w_S is the subsidence or "large-scale" vertical

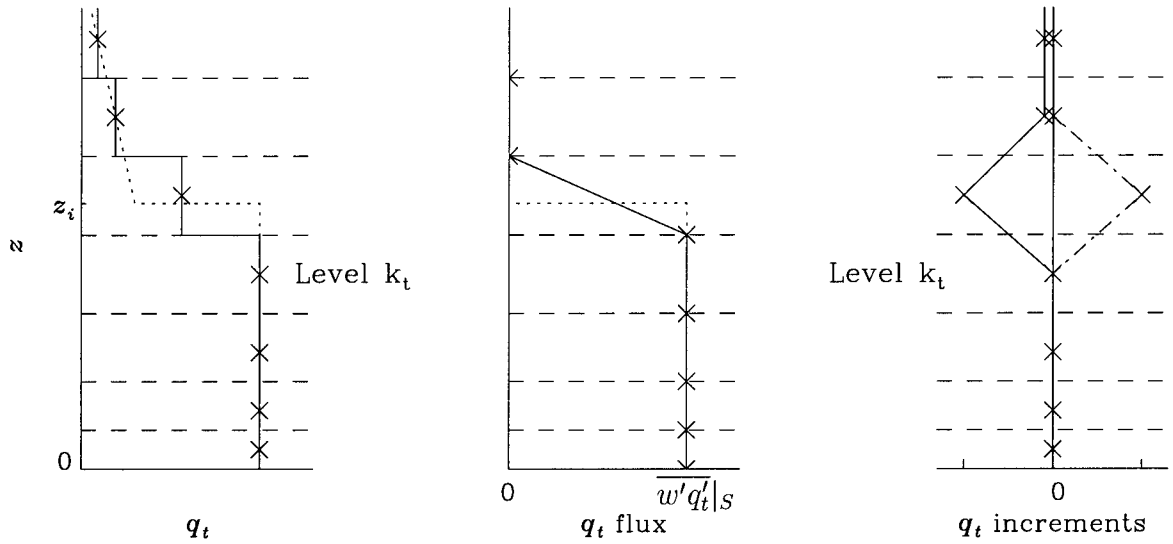

FIG. 1. Idealized profiles of q_t and $\overline{w'q_t'}$, both continuous (dotted lines) and averaged onto a finite-difference grid (solid lines), and associated q_t increments (from subsidence, solid line, and boundary layer processes, dash-dotted line). The grid-level boundaries are shown by the horizontal dashed lines.

velocity (negative if the atmosphere is subsiding) and overbars have from hereon been assumed.

Consider a boundary layer in which buoyant production of turbulence maintains a well-mixed layer. Profiles of conserved quantities, such as q_t, are approximately uniform in height within the boundary layer, as illustrated by the dotted lines in Fig. 1. The boundary layer is capped by an inversion at a height z_i, the evolution of which is governed by

$$\frac{dz_i}{dt} = w_e + w_S|_{z_i}, \tag{4}$$

where w_e is the entrainment rate, generated by turbulent mixing. In Fig. 1, it has been assumed that the entrainment flux, $\overline{w'q_t'}|_{z_i}$, equals the surface flux, $\overline{w'q_t'}|_S$. Thus, both terms on the right-hand side of (3) are negligible *within* the boundary layer and so q_t is approximately constant in time *within* the boundary layer. In Fig. 1, the continuous q_t profile (the dotted line) has been averaged onto a finite-difference grid and increments to q_t on these grid levels (equal to the integral of the continuous increments over each grid level) are also shown. The effect of subsidence is to push the unresolved inversion down and so this appears as a drying in the finite-difference grid level above the boundary layer, denoted level $k_t + 1$. Similarly, the turbulent flux divergence across this grid level (which arises from the entrainment flux at the top of the mixed layer with zero flux above) generates a moistening in level $k_t + 1$. Note that, in this idealization, the subsidence has been chosen such that, at the inversion, it approximately balances the entrainment rate. Thus, the inversion would remain stationary in ''reality'' and, in the finite-difference representation, the increments in level $k_t + 1$ approximately cancel.

A crucial feature of this well-mixed regime in which the entrainment and surface fluxes of q_t are equal is that, as long as the source of turbulent energy remains unaffected, q_t will be constant *within* the boundary layer regardless of whether the boundary layer is deepening or becoming shallower. In other words, q_t *within* the boundary layer knows nothing about whether the large scale is stationary or subsiding.

b. The balance in the SBL scheme

In the SBL scheme used here, the entrainment fluxes are parameterized through the eddy diffusivity, K_h, at the model flux level directly above the top of the mixed layer. The grid level at the top of the mixed layer (denoted level k_t, see Fig. 1) is found by a parcel ascent, as described in Lock et al., and the flux level (or half-level) above is denoted level $k_t + \frac{1}{2}$. The entrainment K_h is specified as $K_h = w_e \Delta_{k_t+1} z$, where Δ_{k_t+1} denotes a finite difference between grid levels $k_t + 1$ and k_t, and the entrainment rate parameterization can be written

$$w_e = \mathrm{TKE}_{fg}/\Delta_{k_t+1} b. \tag{5}$$

Here, TKE_{fg} is a function of the turbulence forcing in the layer and $\Delta_{k_t+1} b$ is the buoyancy strength of the inversion, as measured across grid levels $k_t + 1$ and k_t. It should be noted that, when implemented in the scheme's first-order closure, (5) generates grid-independent entrainment fluxes as long as TKE_{fg} is grid independent. Note also that fluxes within the boundary layer (grid levels $k_t - \frac{1}{2}$ and below) are parameterized through specified eddy diffusivity profiles, K_h, which essentially act to keep the layer well mixed, as discussed in Stevens (2000).

SCM simulations have been performed with the SBL

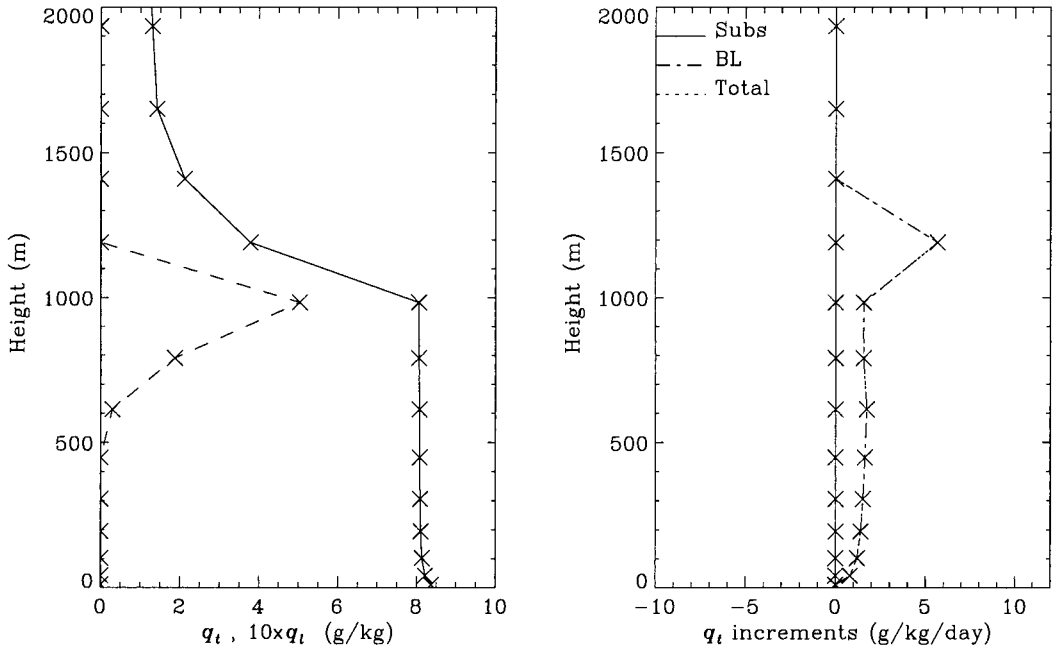

FIG. 2. Profiles from the SCM simulation of the idealized stratocumulus regime without subsidence using the SBL scheme after 1 h: (a) q_t (solid line) and 10 q_l (dashed); (b) increments to q_t—total (dotted line) and that arising from subsidence (solid line) and the boundary layer scheme (dash-dotted line).

scheme that attempt to mimic the simple well-mixed equilibrium stratocumulus regime discussed in section 3a. The model is described in more detail in section 5 and is run here with the shortwave radiation, precipitation, and mass-flux convection schemes switched off. The vertical grid spacing is approximately 200 m around cloud top and the simulations have been run for 1 h with a 10-min time step. This length of integration has been chosen as it is long enough to allow the model to adjust (very slightly) to the initial profiles, but short enough that the turbulence generation (predominantly by cloud-top radiative cooling) is unaffected by the presence of subsidence. The sea surface temperature used in the model's lower boundary condition has been chosen so that the surface flux of q_t approximately matches the entrainment flux diagnosed by the SBL scheme. The entrainment rate determined by the model is approximately 0.3 cm s^{-1} and so z_i would only rise by around 10 m in an hour were $w_S = 0$.

Figure 2 shows the instantaneous profile of q_t and increments to it after 1 h from the SCM simulation without subsidence. Specifying the entrainment flux at level $k_t + ½$ (at 1100 m), with zero fluxes above, generates a flux divergence above the top of the mixed layer that gives a moistening increment in grid level $k_t + 1$, at 1200 m. The slight moistening within the boundary layer results from a surface flux slightly larger than the entrainment flux.

Figure 3 shows the same profiles but from a SCM simulation with an imposed large-scale divergence, $\mathcal{D} = 3 \times 10^{-6}$ s^{-1}, where

$$w_S|_z = -\mathcal{D}z.$$

Thus, $w_S \approx -0.3$ cm s^{-1} at cloud top so that subsidence and entrainment should approximately balance there.

For simplicity, and to avoid the generation of numerical noise, first-order upwind advection is used to calculate the subsidence increments. As can be seen in Fig. 3, the subsidence increments associated with the inversion are spread over the two grid levels spanning the inversion (k_t and $k_t + 1$, at approximately 1000 and 1200 m). This is not specific to first-order upwind advection but quite natural, given the finite-difference representation. Recall that the entrainment flux is specified at grid level $k_t + ½$ and so, as in the simulation without subsidence, the moistening that arises from the flux divergence associated with the inversion appears in level $k_t + 1$. Thus, the entrainment and subsidence increments no longer balance in level $k_t + 1$ as they did in reality, in Fig. 1. In addition, the turbulent mixing scheme within the mixed layer (i.e., that responsible for the fluxes between levels 1 to k_t) is sufficient to mix the subsidence increment at level k_t uniformly over the boundary layer. This results in a net *drying* of the mixed layer, see Fig. 3b, which is to be contrasted with the net *moistening* that occurred in the simulation without subsidence, see Fig. 2b. As described by Lenderink and Holtslag (2000), this is not a problem peculiar to the use of specified eddy diffusivity profiles within the mixed layer. The highest flux level within the mixed layer, $k_t - ½$, is some 200 m below cloud top and so any turbulence scheme would be expected to generate strong turbulent

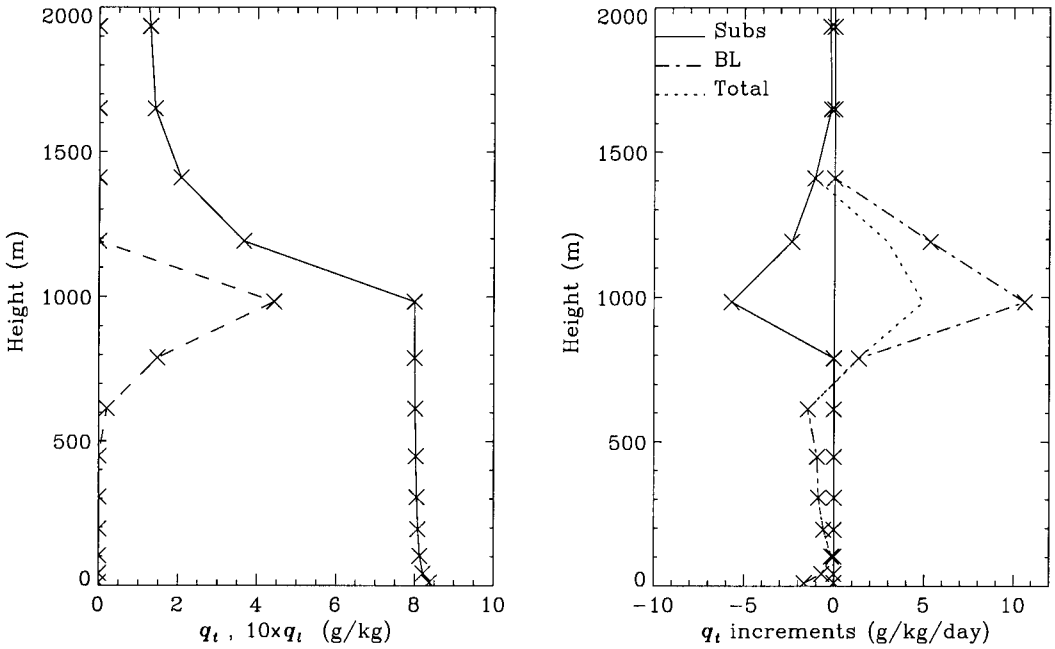

FIG. 3. As in Fig. 2 but from the SCM simulation with subsidence, using the SBL scheme.

mixing there. Thus, inconsistency in the treatment of the inversion between the turbulence scheme and vertical advection leads to a net moistening of levels k_t and $k_t + 1$, and a net drying of the boundary layer. This has the appearence, therefore, of spurious additional entrainment, which was called numerical entrainment by Lenderink and Holtslag.

It has been shown, then, that the numerical representation of entrainment in the Lock et al. boundary layer scheme generates a time evolution of q_t within the mixed layer that is strongly (and erroneously in this simplified regime) dependent on the presence of subsidence. This has been found to be due to the boundary layer scheme using a numerical representation of the inversion that is inconsistent with that used to represent subsidence. It should be noted that the problem is more fundamental than simply the inappropriate assumption of a discontinuous inversion in the Lock et al. entrainment parameterization. Lenderink and Holtslag found the same dependence in their SCM with a 1.5-order *E–l* turbulence closure; while their boundary layer scheme's treatment of the inversion is very different from that in Lock et al., it remains inconsistent with that of the vertical advection scheme.

4. Improving the representation of the inversion

In the previous section it was established that the SBL scheme's treatment of the inversion was seriously inconsistent with that of resolved vertical advection and that this could then lead to the generation of spurious entrainment. A similar problem was discussed in the appendix of Lock (1998), and in more detail in Stevens et al. (1999, their appendix C), where spurious entrainment can be generated from an inconsistent distribution of cloud-top radiative cooling between the inversion grid level and the mixed layer. B. Stevens (2000, personal communication) suggested a framework, also adopted by Grenier and Bretherton (2001), within which the inversion can be treated consistently on a finite-difference grid for all processes. Grenier and Bretherton (2001) tested three methods of representing the inversion. One of these was ''profile reconstruction,'' in which a subgrid inversion structure was diagnosed each time step, simply from the model profile of θ_{vl}. A similar method is used here, as described in the appendix. This subgrid structure can then be used to diagnose a realistic coupling between turbulent, radiative, and advective fluxes.

Working with an SCM, Grenier and Bretherton achieved this by using the subgrid structure to calculate all three of these fluxes in the grid levels adjacent to the inversion. In the context of the idealized stratocumulus simulation discussed in section 3, profile reconstruction would indicate a subgrid inversion somewhere between flux grid levels $k_t + \frac{1}{2}$ and $k_t + \frac{3}{2}$ (between 1100 and 1300 m). Thus, in calculating the advective source term in level k_t, $-w_S \partial q_t / \partial z$, Grenier and Bretherton would essentially use a mixed-layer q_t gradient, because the mixed layer has been diagnosed as extending into the grid level above. While that may be relatively straightforward in a one-dimensional model, interpreting the inversion structure in a three-dimensional GCM could be far more problematic, not least because the profile reconstruction is performed independently in each grid column.

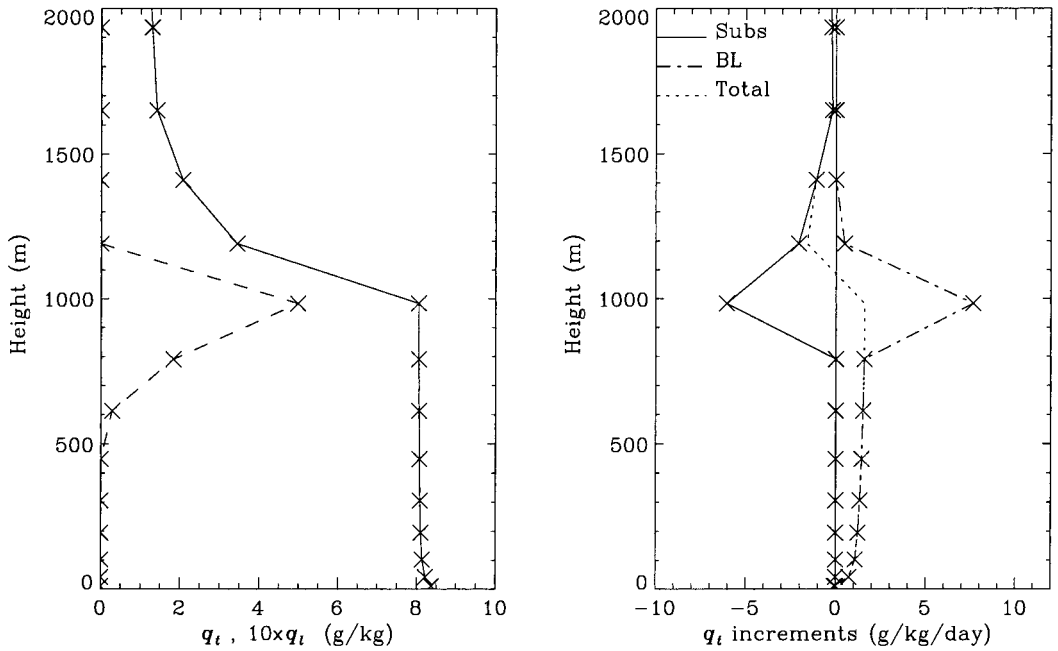

FIG. 4. As in Fig. 3, from the SCM simulation with subsidence, but using the RBL scheme.

An alternative approach, and the one adopted here, is to allow for the distribution of the subsidence and radiative increments between the grid levels spanning the inversion when specifying the parameterized entrainment flux. In that way the inversion is still treated consistently between processes but, in the context of a numerically secure implementation in a GCM, the net result is only an adjustment to the entrainment parameterization. Referring to the idealized stratocumulus simulation discussed in section 3, the specified entrainment flux is reduced to allow for the numerical entrainment implied by the location of a subsidence increment inside the mixed layer, in level k_t (at 1000 m; see Fig. 3b). This is what has been implemented in what will be referred to as the revised boundary layer (RBL) scheme, described below, to give the SCM increments shown in Fig. 4b. Notice how the reduced entrainment flux reduces the moistening from the boundary layer scheme in level $k_t + 1$ (at 1200 m; cf. Fig. 3) so that precisely the same net moistening is generated *within* the boundary layer as was observed in the simulation without subsidence (dotted lines in Figs. 2b and 4b). Thus, the RBL scheme does give a boundary layer evolution that is independent of the presence or absence of subsidence, consistent with the analysis in section 3a.

An additional advantage of diagnosing a subgrid inversion is that is provides a means of more accurately modeling fluxes in thin (relative to a GCM grid) mixed layers, such as decoupled stratocumulus layers. If the parameterized entrainment flux is simply specified at a model flux level then, assuming linear fluxes within the mixed layer, the error in the flux gradient across the layer is $O(\Delta_k z/z_{ml})$, where $\Delta_k z$ is the model grid size and z_{ml} the thickness of the mixed layer. Thus, as z_{ml} approaches $\Delta_k z$, significant errors can be incurred.

The next section describes in detail how the subgrid inversion structure can be used to unify the numerical representation of the inversion in the turbulence, radiation, and subsidence schemes. Note that, in the context of the Lock et al. scheme, these calculations need only be performed if a convective mixed layer (at the top of which entrainment will be parameterized) is diagnosed.

Specifying the entrainment fluxes

Consider first how to specify the model's entrainment fluxes in the absence of subsidence, given a subgrid inversion at a height $z = z_i$ and with a jump in a quantity χ across it of $\Delta\chi$ (note the absence of a subscript to constrast the subgrid profile with grid-level finite differences). If it is assumed that the turbulent fluxes reduce from their extremum at $z = z_i$ (the entrainment fluxes) to zero at $z = h$ a small distance above, and that the rate of change of the inversion strength is negligible, then

$$\mathcal{H}|_{z_i} = -\tilde{w}_e \Delta\theta_\ell + F_{\text{net}}|_h \qquad \overline{w'q_t'}|_{z_i} = -\tilde{w}_e \Delta q_t, \quad (6)$$

where the total heat flux $\mathcal{H} = \overline{w'\theta_\ell'} + F_{\text{net}}$ and $\tilde{w}_e$ is the adjusted entrainment rate (as described toward the end of this section). The net radiative flux, F_{net}, is calculated relative to the base of the mixed layer so that F_{net} there is zero. Note that integrating the thermodynamic equation across the inversion implies $\overline{w'\theta_\ell'}|_{z_i} = -\tilde{w}_e \Delta\theta_\ell + F|_h - F|_{z_i}$. The radiative flux at the top of the subgrid inversion, $F|_h$, is estimated by extrapolating down from $F_{k_t+3/2}$ using the net radiative flux divergence in level k_t

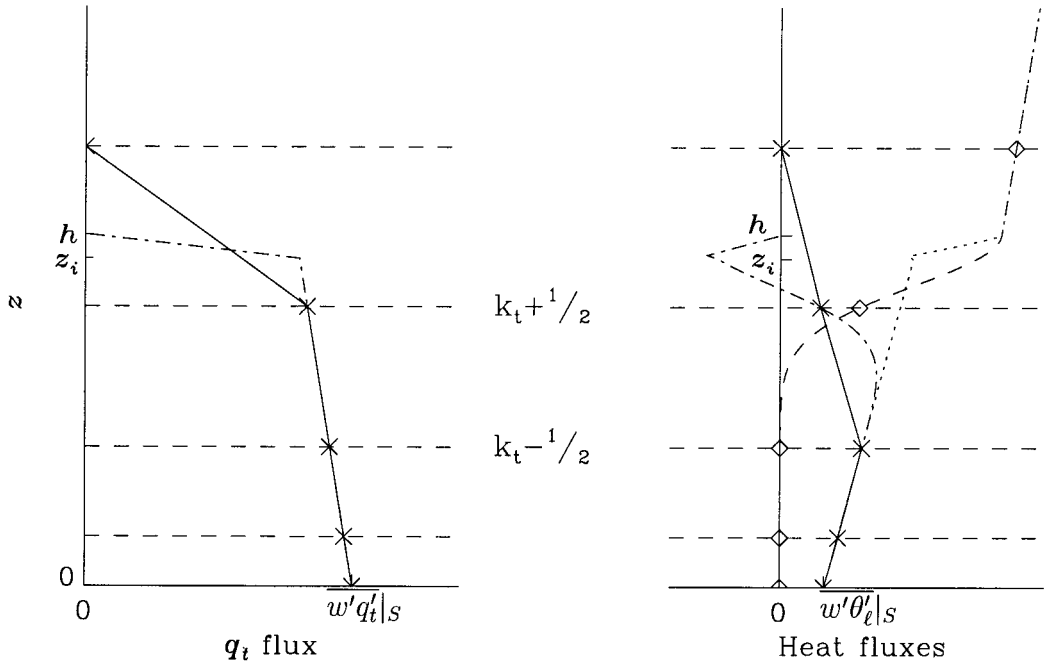

FIG. 5. High-resolution profiles of (a) $\overline{w'q'_t}$ (dash-dotted line) and (b) $\mathcal{H}$ (dotted line), $\overline{w'\theta'_\ell}$ (dash-dotted), and F (dashed). The continuous lines are the turbulent fluxes on the coarse grid indicated by the dashed horizontal lines (assuming identical radiative fluxes, as denoted by the diamonds).

+ 2. Alternatively, the subgrid structure could be used in the model's radiation scheme, but this has not yet been attempted.

In the finite difference model, the entrainment fluxes are imposed nominally at the subgrid inversion height, z_i. Ignoring the flux arising from precipitation, the assumption of a quasi steady-state layer capped by a discontinuous inversion implies that $\mathcal{H}$ and $\overline{w'q'_t}$ will be linear between the surface and z_i. Thus, the required grid-level fluxes (at a height $z_{k_t+1/2}$) can be estimated as

$$\overline{w'\theta'_\ell}|_{z_{k_t+1/2}} = \overline{w'\theta'_\ell}|_S - \frac{z_{k_t+1/2}}{z_i}(\tilde{w}_e\Delta\theta_\ell + \overline{w'\theta'_\ell}|_S - F_{\text{net}}|_h) - F_{\text{net}}|_{z_{k_t+1/2}}$$

$$\overline{w'q'_t}|_{z_{k_t+1/2}} = \overline{w'q'_t}|_S - \frac{z_{k_t+1/2}}{z_i}(\tilde{w}_e\Delta q_t + \overline{w'q'_t}|_S). \qquad (7)$$

This interpolation is illustrated in Fig. 5. The impact of coupling the turbulent flux to the radiative flux profile can be seen in the resulting *positive* $\overline{w'\theta'_\ell}|_{z_{k_t+1/2}}$ in Fig. 5, whereas the SBL implementation of the entrainment parameterization ($-\tilde{w}_e\Delta\theta_\ell$) would give a negative flux. The effect, then, is for the turbulence to warm grid level $k_t + 1$, rather than cool it, because a substantial part of the large radiative cooling in grid level $k_t + 1$ should be mixed down into the boundary layer.

Note that it is not possible to use the same value of K_h to specify the fluxes given by (7), as is done in the SBL scheme (see section 3b). Essentially, this is because $\overline{w'\theta'_\ell}|_{z_{k_t+1/2}}$ includes an explicit balance between the turbulent and radiative fluxes. In addition, because the latter are fixed through the time step, it would be more consistent to assume the entrainment fluxes, (6), are also fixed. Within the implicit numerical scheme used to integrate the equations, therefore, the entrainment fluxes themselves should be specified, rather than entrainment eddy diffusivities.

In order to allow for the long time steps used in GCMs and to allow the balance with subsidence to be generalized to both rising and falling inversions, the parameterization of w_e and the model's subsidence velocity, w_S, are used to calculate z_i at the next time level (denoted z_i^{n+1}). Equally importantly, without a diagnosis of the evolution of z_i, the only way the previous formulation (either in the RBL or SBL schemes) could represent a subsiding inversion was for the inversion diagnosis by the parcel ascent to drop down a grid level. This reliance on a parcel ascent to detect small changes in stability around the inversion makes the previous formulation liable to error and significantly time step dependent.

The proposed solution to these problems, then, is to use the parameterized w_e and the model's $w_S|_{z_i}$ to calculate z_i^{n+1}. Currently, $w_S|_{z_i}$ is found by linear interpolation to z_i and both it and w_e are assumed constant in time. Note first that $z_{k_t+1/2} < z_i < z_{k_t+3/2}$, as described in the appendix. If $z_i^{n+1} < z_{k_t+1/2}$, then the entrainment fluxes [given by (7)] are multiplied by the fraction of the time step that z_i was above $z_{k_t+1/2}$, namely, $(z_i - z_{k_t+1/2})/(z_i - z_i^{n+1})$. As this should imply an inversion

between grid levels $k_t - 1$ and k_t by the end of the time step, the fluxes at level $k_t - ½$ must then also be specified, rather than be determined using the mixed-layer K profiles. These fluxes are given by (7) with $z_{k_t+1/2}$ replaced by $z_{k_t-1/2}$. If $z_i^{n+1} > z_{k_t+3/2}$, the entrainment flux need only be specified at this higher grid level (multiplied by the fraction of the time step that z_i is above $z_{k_t+3/2}$) and the mixed-layer K profiles are extended to level $k_t + ½$. Note that wherever the entrainment fluxes are specified explicitly, the eddy diffusivity is set to zero. Also, the mean value of z_i during the time step is used in (7) in order best to approximate the mean flux gradient across the mixed layer.

It then remains to adjust the entrainment flux, at whatever level it is specified, to allow for any entrainment implied by a subsidence increment in the grid level below. The subsidence increments could be obtained directly in the SCM but in a three-dimensional model (such as a GCM) advection increments can have a significant contribution from the horizontal component. The subsidence increments are calculated, therefore, from the vertical velocity field using first-order upwind advection. This is actually what is used to calculate the increments in the SCM, but it would clearly be preferable to use the model's actual vertical advection algorithm in the GCM (although the errors incurred in this diagnostic calculation should not be very significant). The entrainment fluxes interpolated onto the relevant grid levels are calculated as described above, using an entrainment velocity, $\tilde{w}_e$, in (7) that is reduced to allow for any subsidence increments applied to the grid level below the entrainment flux. To take the case of z_i remaining within level $k_t + 1$ as an example, this reduced entrainment velocity is given by $\tilde{w}_e = w_e + \tilde{w}_S$, with $\tilde{w}_e$ constrained to lie between 0 and w_e, where

$$\tilde{w}_S = -\frac{\Theta_{k_t}^S (z_{k_t+1/2} - z_{k_t-1/2})}{\Delta\theta_\ell}. \tag{8}$$

This calulation of $\tilde{w}_S$ is used (rather than simply the subsidence velocity itself, for example) to ensure that $\overline{w'\theta'_\ell}|_{z_{k_t+1/2}}$ in (7) is reduced by precisely the right amount to compensate for the θ_ℓ subsidence increment in grid level k_t, $\Theta_{k_t}^S$ (at least up to the point where $\tilde{w}_e$ has been reduced to zero). Although not implemented here, $\tilde{w}_S$ could in principle be recalculated using the q_t subsidence increment in (8) when used to limit $\overline{w'q'_t}|_{z_{k_t+1/2}}$ in (7). For first-order upwind advection, however, the two should be very similar because the assumptions underlying the treatment of the inversion grid level imply $\Delta_{k_t+1} q_t / \Delta_{k_t+1}\theta_\ell \approx \Delta q_t / \Delta\theta_\ell$. Finally, note that the result of overestimating the subsidence increment applied below the entrainment flux grid level would only be to reduce the total entrainment generated in the model (potentially to zero).

5. Single-column model results

The SCM used is a one-dimensional (vertical) configuration of the Met Office Unified Model (UM). In addition to the boundary layer parameterization described here, cumulus convection is parameterized using the mass-flux scheme of Gregory and Rowntree (1990). Layer cloud liquid water and cloud fraction are diagnosed from the prognostic and advected model variables, θ_ℓ and q_t, following Smith (1990) and precipitation from layer cloud is as in Senior and Mitchell (1993), a bulk scheme with parameterized autoconversion and accretion. Radiative fluxes are calculated using a general two-stream radiation scheme (Edwards and Slingo 1996). Note that the subgrid inversion structure is currently only used in the boundary layer scheme, although it is intended in the future to extend it to, for example, the cloud scheme.

A number of SCM simulations have been performed to test this scheme. The three presented here were driven by prescribed large-scale divergence and geostrophic winds. For the two stratocumulus simulations, prescribed sea surface temperatures (SST) (with the surface fluxes calculated using Monin–Obukhov similarity theory) were used while surface fluxes were prescribed for the cloud-free simulation. The geostrophic wind was held constant at $(-10, -3)$ m s^{-1} in the stratocumulus simulations and $(10, 0)$ m s^{-1} in the cloud-free simulations. As standard, a 10-min time step is used and there are 14 pressure grid levels below approximately 750 hPa (for a surface pressure of 1020 hPa) with the spacing stretched away from the surface. This is the resolution used when the scheme is implemented in the GCM and gives a grid spacing of around 200 m between 500 and 1500 m, for example.

As described in section 2, and in more detail in Lock et al., both the SBL and RBL schemes can model turbulent mixing in both well-mixed and decoupled stratocumulus-capped boundary layers. In the results that follow, $z_{\rm sml}$ marks the height of the inversion (subgrid for the RBL scheme) capping the $K^{\rm surf}$ profile, $z_{\rm Sc}$ the inversion capping the $K^{\rm Sc}$ profile and $z_{\rm top} = \max[z_{\rm sml}, z_{\rm Sc}]$ (so $z_{\rm top} = z_{\rm sml}$ in well-mixed layers). Recall that if cumulus convection is diagnosed, $z_{\rm sml}$ is set to the height of the LCL.

a. Nocturnal subsiding stratocumulus

The stratocumulus simulation introduced in section 3b has been run for 4 days with an enhanced subsidence rate, $\mathcal{D} = 5 \times 10^{-6}$ s^{-1}, so that the cloud layer should now slowly fall. In order to illustrate more clearly the impact of the revised treatment of entrainment on the cloud, and hence on the boundary layer evolution, the SCM has been run without shortwave radiation and with the mass-flux convection scheme switched off, although all other aspects of the simulation are realistic. Figure 6 shows time–height contour plots of q_ℓ. With the SBL scheme, rather than fall, the cloud dissipates in situ (see Fig. 6a) and only then, once the turbulence source has been removed, does the inversion fall. Continued heating and moistening from the surface cause the grid level

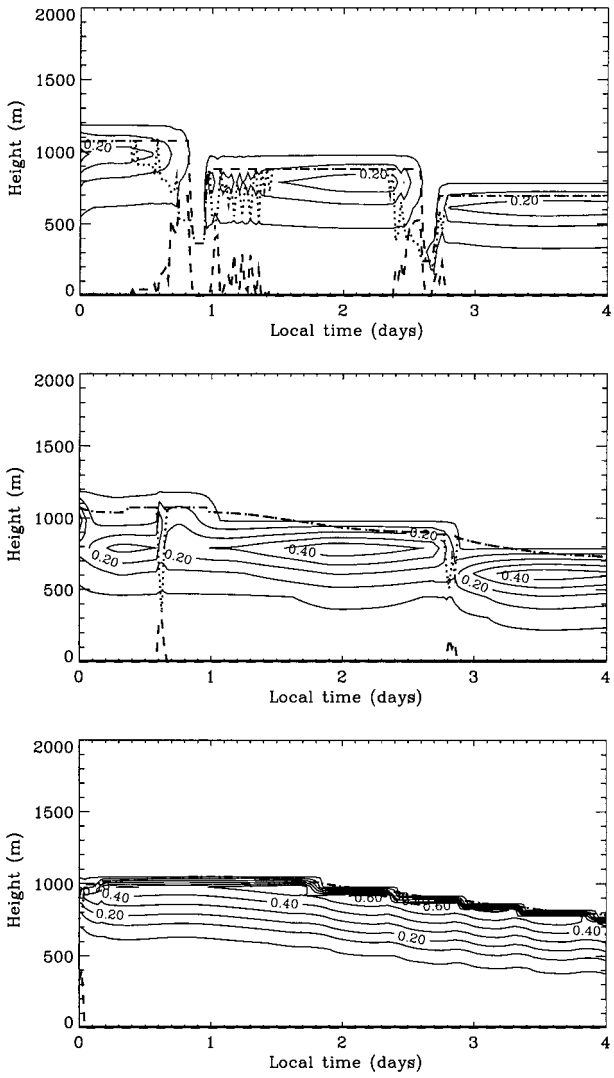

FIG. 6. Time–height contour plots of q_l from standard SCM simulations of nocturnal stratocumulus using (a) the SBL and (b) the RBL scheme. (c) is from the RBL scheme with enhanced vertical resolution. Contour spacing is 0.1 g kg^{-1} with an additional contour at 0.01 g kg^{-1}. The dotted line is z_{sml} and the dashed lines indicate z_{top} and the lower boundary of any well-mixed decoupled cloud layer.

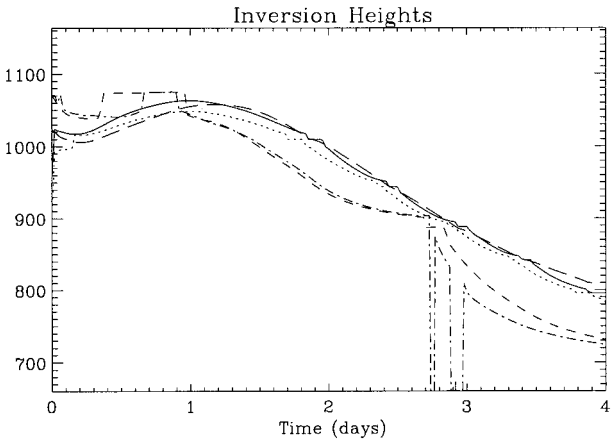

FIG. 7. Time series of z_{top} diagnosed by the RBL scheme as standard (dashed line), with a 30-min time step (dash-dotted) and with enhanced resolution (5-min time step, solid, 15 min time step, dotted) and as predicted by integrating (4) for the high-resolution short time step simulation (long-dashed line).

below to become saturated. Because the old cloud-top grid level still has θ_ℓ and q_t values much closer to the boundary layer values than the free atmosphere, the subsidence increment in the grid level below it is initially quite small and so the cloud persists. As the grid level above the new cloud top gradually dries and warms toward the free-atmospheric values, the numerical entrainment increases and once again causes the cloud to be completely evaporated.

Applying the revised treatment of the inversion described above (the RBL scheme), the cloud layer slowly descends and remains continuous to the end of the simulation (see Fig. 6b), as expected. As was described in section 4, the RBL scheme's representation of the inversion has been made distinct from the model grid. Combined with the fact that the eddy diffusivity profiles are specified continuous functions, this property should ensure a high degree of time step and resolution independence. This can be seen in practice in Fig. 6c, which shows the results from the RBL scheme with enhanced (~50 m) resolution (with a 15-min time step). In addition, Fig. 7 shows that the diagnosed inversion height (z_{top}, diagnosed independently every time step) moves at a rate reasonably close to that predicted by integrating (4) for the high-resolution (short time step) simulation, independent of both resolution and time step to a high degree.

Recall that in all these simulations decoupling of the cloud layer from the surface is diagnosed when the ratio of consumption to production of TKE by buoyancy exceeds a magnitude of 0.1. Its occurrence in these simulations [made apparent in Fig. 6 by z_{sml} (dotted line) falling below z_{top} (upper dashed line)] is entirely erroneous. It occurs when there is insufficient resolution of the buoyancy production due to condensation in the cloud layer, as calculated by (2). This happens with the SBL scheme as the cloud dissipates. With the RBL scheme, it occurs solely at the standard resolution (in Fig. 6b) and even then only as the cloud layer rises or falls. This is because, in the process, the number of grid levels with significant q_ℓ falls from a minimal 2 to just a single level. Note that the decoupling resulting from this lack of resolution appears to occur more readily with a longer time step, as can be seen in Fig. 7 (dash-dotted line) with the sudden but brief drop in z_{top} toward the end of day 2. This may be due to the ''serial'' method of time advancement used in the UM, in which the increments calculated by each parameterization scheme are added to the model fields before those fields are passed on to the next scheme. In particular, the radiative fluxes are calculated just after the subsidence increments

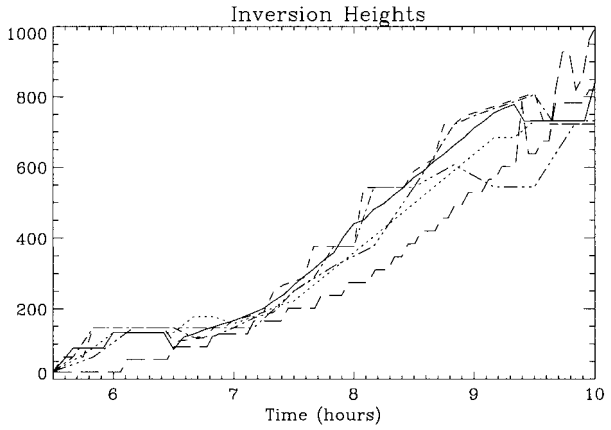

FIG. 8. Time series of inversion height from the cloud-free mixed-layer case: from the LES (long-dashed lines) and from the SCM with enhanced resolution (with 5-min, solid line, and 10-min time step, dotted line) and standard resolution (with 5-min, dashed, 10-min, dash-dotted, and 20-min time step, dash-dot-dot-dotted line).

have been added and, in this simulation, these can be sufficient to evaporate a significant fraction of the cloud in a half-hour time step, significantly reducing the cloud-top radiative cooling of the cloud layer and, therefore, the strength of the turbulent mixing.

b. A rapidly deepening cloud-free mixed layer

This case is an early morning transition over land from a shallow nocturnal boundary layer to a rapidly deepening cloud-free convective boundary layer. It is based on data from the Southern Great Plains Atmospheric Radiation Measurement site (R. Cederwall 1999, personal communication) and develops into a shallow cumulus-capped boundary layer, as described in Lock et al. (2000), although this part of the simulation will not be described since the interaction with the mass-flux convection scheme is not being discussed here. The simulation has prescribed surface fluxes for a diurnal cycle, a fixed geostrophic wind of 10 m s^{-1}, and very weak prescribed large-scale and radiative forcing. As there is no significant large-scale subsidence, this simulation is presented only to illustrate the behavior of the subgrid inversion height diagnosis and entrainment parameterization in a rapidly deepening boundary layer. A three-dimensional large eddy simulation (LES), using the model described in Brown (1999) with 40-m vertical by 60-m horizontal gridpoint spacing, has been performed with the same forcing and initial profiles, to give some indication of how well the SCM is performing. Figure 8, then, shows the inversion height diagnosed by the RBL scheme at standard resolution with 5-, 10-, and 20-min time steps and with enhanced vertical resolution with 5- and 10-min time steps. The dashed lines are inversion height diagnostics from the LES (the height of the buoyancy flux minimum and, after 9.5 h, cloud top).

The agreement with the LES in Fig. 8 is quite reasonable (particularly since the entrainment parameterization has not been ''tuned'' to this case) but, more importantly, there appears to be a high degree of numerical convergence, both with time step and resolution. The stepping visible particularly in the shorter time step simulations at the coarser resolution (dashed and dash-dotted lines) occurs when the subgrid inversion is diagnosed below the inversion grid level identified by the parcel ascent; when this happens the inversion is set to be near the top of the grid level below, as discussed in the appendix. Thus, the subgrid inversion diagnosis appears to be acting to alleviate potential time step dependence arising from the parcel ascent mixed-layer diagnosis. Note also that the dips in z_{sml} after 9 h in Fig. 8 occur when cumulus convection is diagnosed by the scheme and z_{sml} is set to the height of the LCL. This happens slightly earlier in the standard resolution simulation with a 30-min timestep (dash-dotted line) but the timing of the other simulations is very close to the first appearance of cumulus clouds in the LES.

c. Stratocumulus to trade cumulus transition

This simulation illustrates the transition from well-mixed stratocumulus to trade cumulus that occurs in the subtropics as air moves over a progressively warmer sea surface and subsidence weakens. The simulation is based on that described in Bretherton et al. (1999) which was driven by the SST and large-scale divergence observed in the first Atlantic Stratocumulus Transition Experiment (ASTEX) Lagrangian experiment, which took place near the Azores (see de Roode and Duynkerke 1997). Figure 9 shows the time evolution of q_l and the mixed-layer boundaries for the standard resolution SBL and RBL simulations. Qualitatively the results are quite similar, with the stratocumulus layer rising and cumulus forming underneath. The cloud is significantly thinner with the SBL scheme, though, and the liquid water path (LWP, calculated here simply by integrating the model's q_l profile) is underestimated compared with the observations, as can be seen in Fig. 10. This can again be attributed to the excessive warming and drying of the cloud layer due to the combined parameterized and numerical entrainment with the SBL scheme. In this case the problem is exacerbated by the resulting weaker cloud-top driven turbulent mixing being unable to couple the cloud layer to the surface mixed layer (which is moister and has a lower potential temperature) around day 170. Note from Fig. 10 that there is again little resolution or time step dependence for the RBL scheme, at least until day 171 when cumulus convection (not performed by the boundary layer scheme) is present. During this latter half of all the simulations, the decoupled cloud layer has a greater LWP in the model compared to the observations, although there were no actual observations made between days 170.8 and 171.4. The interaction with the mass-flux convection scheme is an

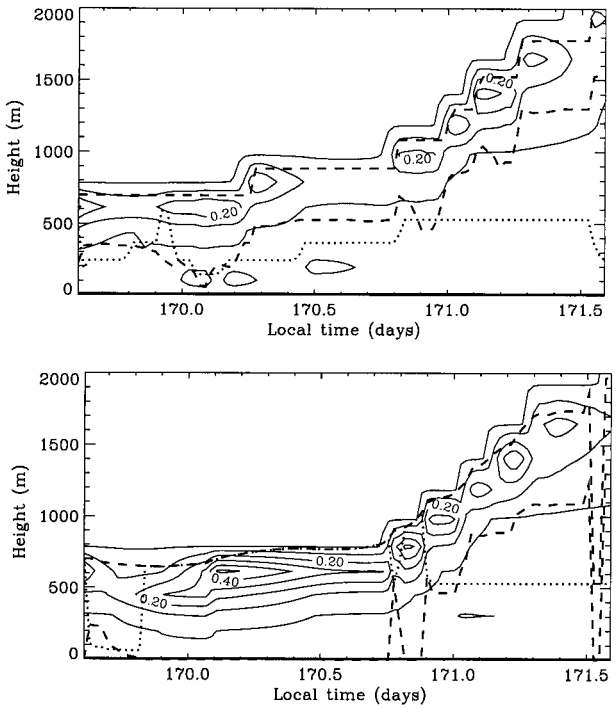

FIG. 9. As Fig. 6 but from SCM simulations of the first ASTEX Lagrangian experiment using (a) the SBL and (b) the RBL scheme.

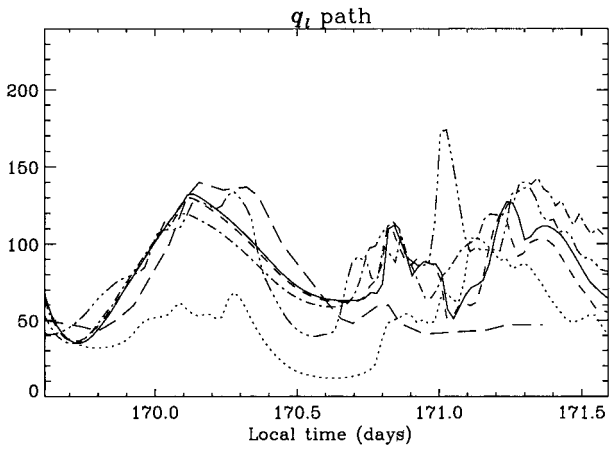

FIG. 10. Liquid water path from observations made during the first ASTEX Lagrangian experiment (long-dashed line) and from the SCM simulations using the SBL with a 10-min time step (dotted line) and the RBL scheme (continuous, dashed and dash-dotted lines) with 5-, 10-, and 30-min time steps, respectively, and with enhanced resolution and a 10-min time step (dash-dot-dot-dotted).

outstanding issue with this boundary layer scheme but it is hoped that it will be addressed by work currently in progress.

6. GCM results

The GCM used here is a version of the Met Office UM, a gridpoint atmospheric GCM. The UM has a finite difference representation of the dynamical, thermodynamic, and mass conservation equations for which the effects of unresolved processes are calculated by a set of physical parameterization schemes. A new version of the UM is used in this study that includes a semi-Lagrangian, semi-implicit numerical treatment of the dynamics, a staggered height-based vertical grid in which the momentum variables are offset in the vertical from the thermodynamic variables, and a different method of time advancement from that used in the SCM here. This last difference addresses the problems discussed in section 5a by passing balanced fields from the end of the previous time step to the boundary layer and radiation schemes. As discussed in Martin et al. (2000), this new version of the UM (which is currently under development) has been found to generate stratocumulus-capped boundary layers over the eastern subtropical oceans that are deeper and have larger cloud amounts compared to the standard UM, although these are still underestimated compared to climatologies. The reasons for this have not yet been isolated. The intention here, however, is only to demonstrate the operation of this revised boundary layer scheme in the more challenging context (compared to an SCM) of a fully three-dimensional atmospheric model, and so the details of the rest of the model should be relatively unimportant. The new version of the UM is used, however, under the assumption that some aspect of the previous version is detrimental to the persistence of subtropical stratocumulus and this might mask any improvement to the boundary layer scheme. There have been some changes to the other parameterization schemes described in Martin et al. (2000), but these have been found to have little impact on the model boundary layer in these regions.

The model has been run with a horizontal resolution of 2.5° latitude by 3.75° longitude (giving a gridpoint spacing of about 300 km in the subtropics) and the same vertical resolution as in the standard SCM simulations. Two simulations were performed, forced by observed sea surface temperatures (prepared for the Atmospheric Model Intercomparison Project; see Gates 1992) from December 1978 for 9 months. One had the SBL and the other the RBL scheme, both as described here.

To illustrate the behavior of the diagnosed subgrid inversion in the GCM, Fig. 11 shows time series (with instantaneous data taken every 2 h or four time steps) during July, of total cloud fraction, LWP, z_{top} and z_{sml} from the simulation with the RBL scheme (continuous lines) and SBL scheme (dotted lines) from the grid point nearest 32°N, 123°W, roughly in the middle of the Californian stratocumulus region. Notice how the rise and, most importantly, the fall of the inversion capping the cloud (z_{top}) is captured with the RBL scheme (solid line in Fig. 11c)—both a weak diurnal cycle and larger-amplitude variations covering several model grid levels over periods of several days—all without destroying the cloud sheet. With the SBL scheme (dotted lines), the inversion is tied to the model grid but, crucially, z_{top}

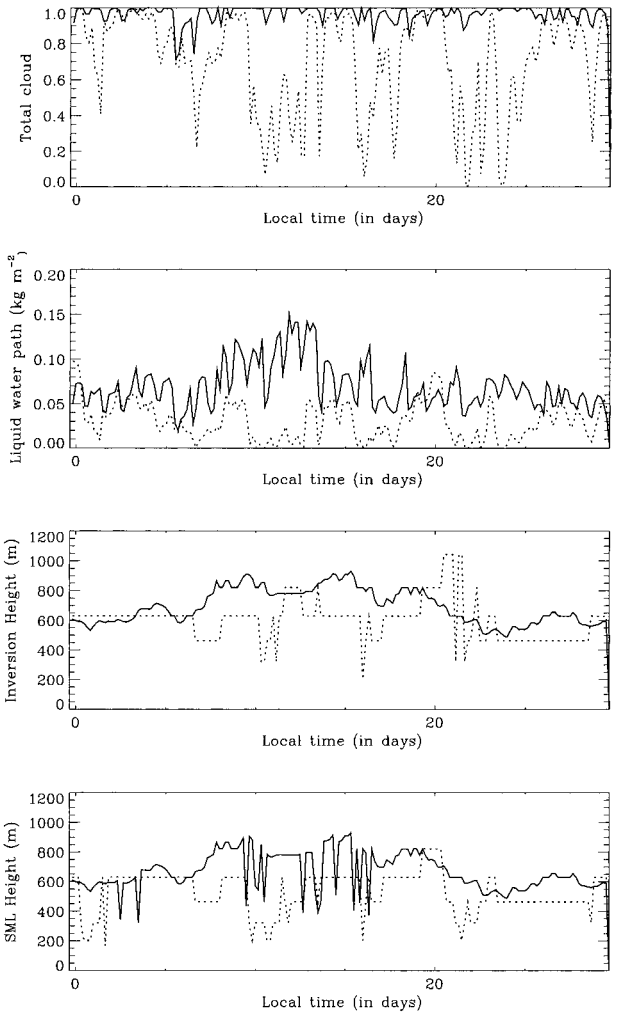

FIG. 11. Time series from July 1979 of (a) total cloud fraction, (b) LWP (kg m^{-2}), (c) z_{top}, and (d) z_{sml} from the GCM simulations with the RBL (solid lines) and SBL (dotted lines) boundary layer schemes from the grid point nearest 32°N, 123°W.

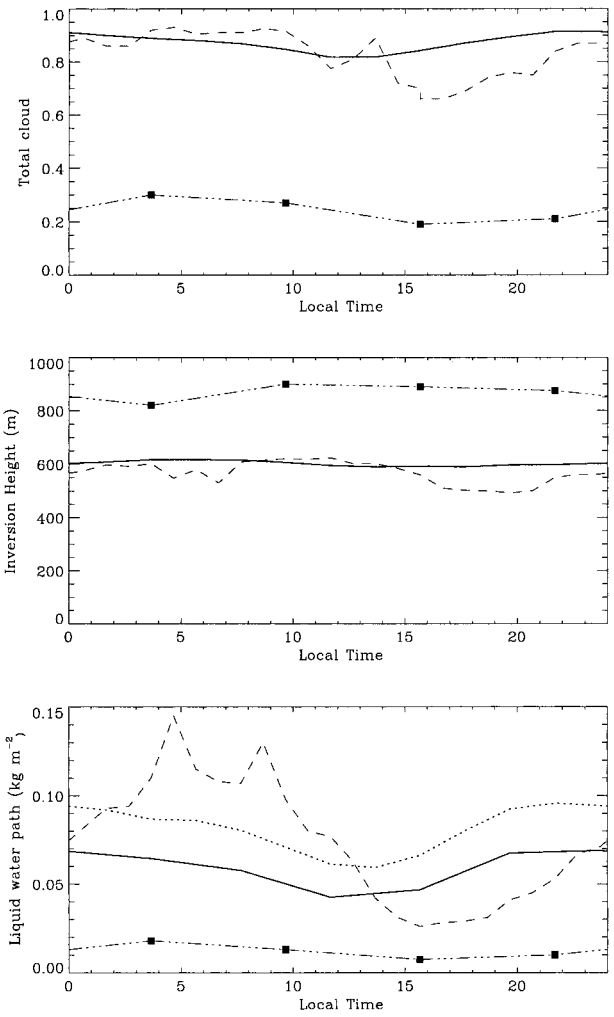

FIG. 12. Diurnally averaged time series of (a) large-scale cloud amount, (b) inversion height, and (c) LWP from the FIRE I observations (dashed lines), the RBL climate simulation (solid lines; the dotted line LWP includes a contribution from the subgrid inversion, as described in the text) and ERA (dash-dot-dot-dotted lines).

never falls without the cloud sheet breaking up (i.e., the LWP falling close to zero, as on days 6, 10, 16, etc.). Thus, the unphysical behavior seen in the SCM studies appears to be reproduced in the GCM. Correcting the error leads to an increase in mean seasonal cloud cover from around 0.6 with the SBL to 0.8 with the RBL scheme, becoming closer to observations in this region. Similar increases are seen in the other subtropical stratocumulus areas. The continuity of z_{top} suggests the RBL scheme is working robustly in the GCM—and examination of time series in other parts of the world, such as the diurnal cycle over land (as in section 5b), support this view—but a more thorough examination, in more complex synoptic situations, for example, is needed to confirm this.

A more detailed comparison of the RBL simulation can be made with observations compiled from the First International Satellite Cloud Climatology Project Regional Experiment I (FIRE I) campaign off the coast of California in July 1987 by Duynkerke and Teixeira (2001). Figure 12 shows time series of the average diurnal variation of inversion height, cloud fraction, and liquid water path from the observations, the European Centre for Medium-Range Weather Forecasts reanalysis (ERA), and the RBL simulation. As for the ERA data in Duynkerke and Teixeira, the RBL data is an average over the area between 28° and 34°N and 119° and 125°W, which amounts to four grid points (all over sea) at this resolution of the UM (less than half the resolution of ERA). It should be noted, however, that the RBL data is an average over July 1979, although this is unlikely to affect the results significantly. Figure 12 suggests the RBL stratocumulus cloud (solid lines) has a realistic total cloud fraction and inversion height. The LWP, as calculated from the model's q_l field (solid line in Fig.

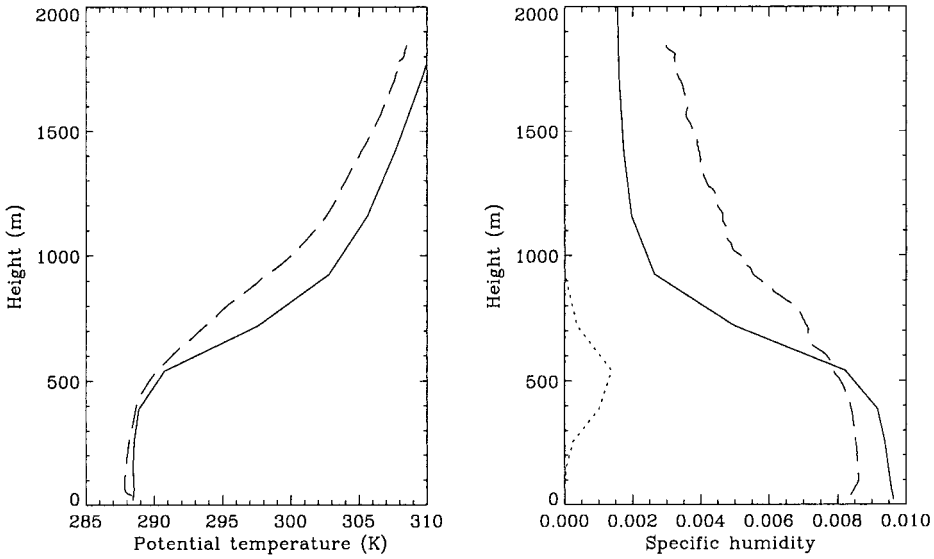

FIG. 13. Averaged profiles of (a) θ and (b) q_v from the FIRE I observations (dashed lines) and the RBL simulation for July 1979 from the area defined in the text (continuous lines). The dotted line in (b) is 10 q_l from the simulation.

12c), would appear to be significantly underestimated, at least overnight. However, the dotted line in Fig. 12c is calculated by extrapolating the liquid water profile adiabatically up to the subgrid inversion height, z_i. This purely diagnostic quantity is significantly larger and therefore closer to the observed LWP at night but is then too large during the day. For both diagnostics, then, the diurnal cycle is too weak. It also appears more strongly linked to the solar forcing than it is in the observations. The cause of these problems with the LWP is not yet known but they may be linked to a lack of daytime decoupling in the model compared to the observations. Decoupling was observed almost daily during FIRE I but the time series of z_{top} and z_{sml} in Figs. 11c and 11d indicate that only on about one-third of the days does the boundary layer decouple (z_{sml} drop lower than z_{top}).

It is not yet clear whether this lack of decoupling is a resolution problem: in the vertical there are only six grid levels below 600 m (and these are concentrated toward the surface) and decoupling appears more prevalent in Fig. 11 when the inversion is higher, during days 9–17. In terms of horizontal resolution, the observations were made on San Nicolas Island, which is very close to the coast of California, and it is not clear how representative these observations are of the model area used for comparison. Alternatively, it could indicate a deficiency in the parameterization of the vertical extent of the eddy diffusivity profiles. As was discussed in section 2, this parameterization is based on the buoyancy flux diagnosed from the model's thermodynamic profiles and so cannot explicitly force decoupling. Finally, the impact of including knowledge of the subgrid inversion in the model's cloud diagnosis (i.e., of increasing the model's LWP from the dotted to the solid line in Fig. 12c) is unknown, although it is discussed further below.

Figure 13 shows the mean profiles of θ and specific humidity, q_v, from the FIRE I observations (dashed lines, reproduced from Duynkerke and Teixeira) and the RBL simulation from the same area as in Fig. 12 (solid lines, for July 1979). Also shown in Fig. 13b is the model average q_l profile, which shows a realistic looking increase with height in the mixed layer. The good agreement for the mixed-layer θ profile is encouraging. Given that the boundary layer in this region is approximately in equilibrium with the sea surface temperature (prescribed in the model), this reinforces the agreement seen in the cloud-top height in Fig. 12. Note that Duynkerke and Teixeira thought the unstable layer near the ground in the observations was probably due to the fact that they were made over land, which may influence the profile close to the ground. Above the mixed layer, the model appears too warm and too dry. Potentially this could indicate an error in the model dynamics or it could be due to the different year in the model compared to the observations. However, it is as likely to be a horizontal-resolution problem, given the summertime land grid points adjacent to those in this diagnostic area. The excess q_v in the model of about 1 g kg^{-1} throughout the depth of the mixed layer would appear to be significant, even given the marginally warmer θ, in view of the otherwise reasonably realistic cloud layer. One possible reason is that the model cloud scheme is still tied to the model grid. When the subgrid inversion is somewhere in the middle of a grid level (as it will be for a significant proportion of the time; see Fig. 11c), the model's cloud scheme is unlikely to diagnose any

cloud in the inversion grid level because air at that level will be a mixture of the moist boundary layer air and the often very dry air from the free troposphere. As the grid size is approximately 200 m, the model can therefore not ''see'' the top 100 m of most cloud sheets most of the time. Because the entrainment rate is strongly dependent on the presence of cloud (via the radiative forcing), a lack of cloud could imply a reduction in entrainment that would lead to a moistening of the boundary layer. This argument is then at least consistent with the excess q_v in the model compared to the observations. It is intended to test passing the subgrid inversion structure to the cloud scheme in the near future.

It should be noted that, while the SBL scheme has a new diagnosis of decoupling from that described in Lock et al., its GCM simulation of the subtropical stratocumulus areas showed no significant improvement. Indeed, a further simulation was performed with the complete RBL scheme except that no compensation was made for the numerical entrainment [i.e., with $\tilde{w}_S \equiv 0$ in (8) so that the full entrainment fluxes were implemented], and that also showed no significant improvement in cloud amounts over the original Lock et al. scheme. Therefore, while the subgrid inversion diagnosis and the associated direct interface with the radiative fluxes [through (7)] may improve the time evolution of simulations, it is accounting for the problem of numerical entrainment that improves the model's stratocumulus climatology.

Also shown in Fig. 12 are the equivalent time series from ERA (reproduced from Duynkerke and Teixeira), which, despite the higher horizontal resolution and being from analyses, still show the severe deficit of stratocumulus more typical of current GCMs.

7. Conclusions

Problems have been identified in the formulation of the Lock et al. (2000) boundary layer scheme. These are associated with the representation of the inversion and the entrainment across it, and the problems are particularly severe in an environment that is subsiding. It has been demonstrated in SCM tests how these can seriously affect the persistence of stratocumulus in the model. That the same problem was first observed by Lenderink and Holtslag (2000) with their *E–l* closure, a significantly different boundary layer scheme, suggests it may be widespread among GCM boundary layer mixing schemes. A correction has been proposed for the Lock et al. scheme in which a discontinuous inversion is diagnosed from the mean thermodynamic profiles every time step. This then allows the parameterized turbulent entrainment flux to be made consistent with the advective and radiative fluxes.

This revised boundary layer scheme has demonstrated a much improved representation of stratocumulus-capped boundary layers not only in SCM tests but also in a climate-resolution GCM. In the latter, the semipermanent subtropical stratocumulus sheets are seen to exhibit realistic-looking behavior and cloud amounts far closer to observed climatologies than many previous GCMs, including the ERA ''climatology.'' Further work will allow the subgrid inversion diagnosis to directly influence the model's cloud field and thence the radiative fluxes.

Acknowledgments. I would like to thank Bjorn Stevens for his clear comments regarding the underlying motivation of this scheme and Peter Duynkerke for supplying the FIRE observations.

APPENDIX

Diagnosis of a Subgrid Inversion

Grenier and Bretherton (2001) used the profile of θ_{vl} to diagnose the height of a discontinuous inversion because it is approximately conserved under adiabatic vertical motion and is equal to the virtual potential temperature, θ_v, in the absence of cloud. This latter property should ensure it is monotonically increasing with height in the statically stable free troposphere of a GCM (and if it is not, this calculation is not performed).

Having identified the model grid level at the top of the well-mixed layer, level k_t, using a parcel ascent (as described in Lock et al. 2000), the grid level above is designated the inversion level within which the diagnosis of a subgrid z_i will be made. If it assumed that θ_{vl} in grid level $k_t + 1$ represents a cell-average value, then z_i can be calculated by assuming that the integral of θ_{vl} over level $k_t + 1$ for the model and for a profile with a discontinuous inversion at z_i are equal, as illustrated by the hatched areas in Fig. A1. To calculate the integral of the discontinuous profile, the lapse rate of θ_{vl} between levels $k_t - 1$ and k_t, γ^{ML}, is extended up to z_i, while the stable lapse in the free atmosphere, between levels $k_t + 2$ and $k_t + 3$, γ^{FA}, is extrapolated down. Equating these areas gives a quadratic equation in $\Delta z_{\mathrm{disc}} = z_{k_t+3/2} - z_i$, where the fractional subscript denotes the height of the half-level, which can be written

$$a(\Delta z_{\mathrm{disc}})^2 + b\Delta z_{\mathrm{disc}} + c = 0. \tag{A1}$$

The coefficients are given by

$$\begin{aligned} a &= 0.5(\gamma^{\mathrm{FA}} - \gamma^{\mathrm{ML}}) \\ b &= -[(\theta_{v\ell})_{k_t+2} - \gamma^{\mathrm{FA}}(z_{k_t+2} - z_{k_t+(3/2)})] \\ &\quad + [(\theta_{v\ell})_{k_t} + \gamma^{\mathrm{ML}}(z_{k_t+(3/2)} - z_{k_t})] \\ c &= (z_{k_t+(3/2)} - z_{k_t+(1/2)}) \\ &\quad \times \{(\theta'_{v\ell})_{k_t+1} - [(\theta_{v\ell})_{k_t} + \gamma^{\mathrm{ML}}(z_{k_t+1} - z_{k_t})]\}. \end{aligned}$$

Clearly, care must be taken to ensure that z_i is not only well defined but also sensible (e.g., as a rising inversion encounters more or less stable regions above). If $b > 0$ this suggests the estimated lapse rates are inappro-

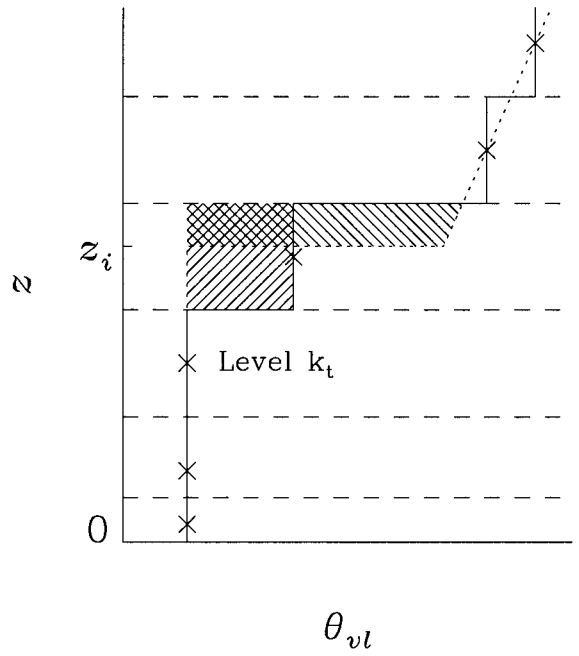

FIG. A1. Schematic illustrating the assumptions behind the diagnosis of z_i.

priate and these are therefore set to zero and (A1) is recalculated. The case $c < 0$ suggests the grid level designated as the inversion level should have been considered as part of the mixed layer and so z_i is set to be fractionally below $z_{k_t+3/2}$ (i.e., as high as possible without attempting to diagnose a subgrid z_i in grid level $k_t + 2$). If $b^2 - 4ac < 0$ the quadratic equation has no real roots. In this instance z_i is set to fractionally below $z_{k_t+1/2}$ and k_t (and therefore the eddy diffusivity profiles) is lowered a level. In addition, from variations seen in z_i during simulations, the error in Δz_{disc} is estimated to be around 10% of the vertical grid spacing, $\Delta_k z$. Accordingly, if z_i is diagnosed as being less than $z_{k_t+1/2} + 0.1\Delta_k z$, k_t is lowered a level and z_i is set fractionally below $z_{k_t+1/2}$. This small distance below the grid level is taken to be $(\Delta t/2) \times 10^{-4}$ so that, were a small rate of rise of z_i (of 10^{-4} m s^{-1}, say) to be diagnosed, then z_i would spend at least half the time step (of length Δt) in the next grid level up. The specified fluxes would then contribute significantly to that grid level's evolution. Conversely, if z_i is subsiding, this technique allows the inversion to drop down a level without requiring this to be done by the initial parcel ascent. This aspect is discussed further in section 4a.

Having calculated z_i, the discontinuous jumps in θ_l and q_t can be calculated from similar integral assumptions. For example,

$$\Delta q_t = [(q_t)_{k_t+1} - (q_t)_{k_t}]\frac{z_{t+(3/2)} - z_{k_t+(1/2)}}{z_{k_t+(3/2)} - z_i}. \quad \text{(A2)}$$

Note that the lapse rate above the inversion has been ignored as there is no guarantee of monotonicity in q_t in the atmosphere above the inversion. In addition, (A2) will become increasingly inaccurate as z_i tends to $z_{k_t+3/2}$ [and $(q_t)_{k_t+1}$ approaches $(q_t)_{k_t}$]. Consequently, if the fraction on the right-hand side of (A2) is greater than 10, double grid-level jumps are used [i.e., $\Delta q_t = (q_t)_{k_t+2} - (q_t)_{k_t}$]. The entrainment parameterization requires a value of the cloud-top q_l, both to quantify the strength of any buoyancy reversal and to calculate the buoyancy jump across the inversion, Δb. This cloud top q_l is estimated by extrapolating $(q_l)_{k_t}$ from z_{k_t} to z_i using the adiabatic lapse rate.

As described in section 2, the Lock et al. scheme is capable of diagnosing decoupled stratocumulus mixed layers, in addition to layers that are well mixed to the surface. All these calculations, then, are performed to diagnose the subgrid structure of both types of layer's capping inversions.

Note that the use of $\Delta\theta_l$ and Δq_t rather than the grid-level jumps should greatly improve the accuracy of the calculation of the buoyancy reversal term in the entrainment parameterization, particularly when the inversion is moving up or down a grid level, because for this term TKE_{fg} in (5) is a function of Δb.

REFERENCES

Bretherton, C. S., S. K. Krueger, M. C. Wyant, P. Bechtold, E. van Meijgaard, B. Stevens, and J. Teixeira, 1999: A GCSS boundary layer cloud model intercomparison study of the first ASTEX Lagrangian experiment. *Bound.-Layer Meteor.*, **93,** 341–380.

Brown, A. R., 1999: The sensitivity of large-eddy simulations of shallow cumulus convection to resolution and subgrid model. *Quart. J. Roy. Meteor. Soc.*, **125,** 469–482.

de Roode, S., and P. G. Duynkerke, 1997: Observed Lagrangian transition of stratocumulus into cumulus during ASTEX: Mean state and turbulence structure. *J. Atmos. Sci.*, **54,** 2157–2173.

Duynkerke, P. D., and J. Teixeira, 2001: Comparison of the ECMWF reanalysis with FIRE I observations: Diurnal variation of marine stratocumulus. *J. Climate*, **14,** 1466–1478.

Edwards, J., and A. Slingo, 1996: Studies with a flexible new radiation code. I: Choosing a configuration for a large-scale model. *Quart. J. Roy. Meteor. Soc.*, **122,** 689–720.

Gates, L. W., 1992: AMIP: The Atmospheric Model Intercomparison Project. *Bull. Amer. Meteor. Soc.*, **73,** 1962–1970.

Gregory, D., and P. R. Rowntree, 1990: A mass flux scheme with representation of cloud ensemble characteristics and stability-dependent closure. *Mon. Wea. Rev.*, **118,** 1483–1506.

Grenier, H., and C. S. Bretherton, 2001: A moist PBL parameterization for large-scale models and its application to subtropical cloud-topped marine boundary layers. *Mon. Wea. Rev.*, **129,** 357–377.

Holtslag, A. A. M., and B. A. Boville, 1993: Local versus nonlocal boundary-layer diffusion in a global climate model. *J. Climate*, **6,** 1825–1842.

Lenderink, G., and A. A. M. Holtslag, 2000: Evaluation of the kinetic energy approach for modeling turbulent fluxes in stratocumulus. *Mon. Wea. Rev.*, **128,** 244–258.

Lock, A. P., 1998: The parametrization of entrainment in cloudy boundary layers. *Quart. J. Roy. Meteor. Soc.*, **124,** 2729–2753.

——, A. R. Brown, M. R. Bush, G. M. Martin, and R. N. B. Smith, 2000: A new boundary layer mixing scheme. Part I: Scheme description and single-column model tests. *Mon. Wea. Rev.*, **128,** 3187–3199.

Martin, G. M., M. R. Bush, A. R. Brown, A. P. Lock, and R. N. B. Smith, 2000: A new boundary layer mixing scheme. Part II:

Tests in climate and mesoscale models. *Mon. Wea. Rev.*, **128,** 3200–3217.
Senior, C. A., and J. F. B. Mitchell, 1993: Carbon dioxide and climate: Impact of cloud parametrization. *J. Climate*, **6,** 393–418.
Smith, R. N. B., 1990: A scheme for predicting layer clouds and their water content in a general circulation model. *Quart. J. Roy. Meteor. Soc.,* **116,** 435–460.
Stevens, B., 2000: Quasi-steady analysis of a PBL model with an eddy-diffusivity profile and nonlocal fluxes. *Mon. Wea. Rev.*, **128,** 824–836.
——, C.-H. Moeng, and P. P. Sullivan, 1999: Large-eddy simulations of radiatively driven convection: Sensitivities to the representation of small scales. *J. Atmos. Sci.*, **56,** 3963–3984.
Turton, J. D., and S. Nicholls, 1987: A study of the diurnal variation of stratocumulus using a multiple mixed layer model. *Quart. J. Roy. Meteor. Soc.,* **113,** 969–1009.